Journal of Power Sources 199 (2012) 395–401

Contents lists available at SciVerse ScienceDirect

Journal of Power Sources

journal homepage: www.elsevier.com/locate/jpowsour

Enhanced high-current capacitive behavior of graphene/CoAl-layered double hydroxide composites as electrode material for supercapacitors

Luojiang Zhang[a], Xiaogang Zhang[a,*], Laifa Shen[a], Bo Gao[a], Liang Hao[a], Xiangjun Lu[a], Fang Zhang[a], Bing Ding[a], Changzhou Yuan[b]

[a] College of Material Science and Engineering, Nanjing University of Aeronautics and Astronautics, Nanjing 210016, PR China
[b] School of Materials Science and Engineering, Anhui University of Technology, Ma'anshan 243002, PR China

ARTICLE INFO

Article history:
Received 12 June 2011
Received in revised form 7 September 2011
Accepted 16 October 2011
Available online 20 October 2011

Keywords:
Graphene
Layered double hydroxide
Capacitive behavior
Supercapacitor

ABSTRACT

Graphene nanosheets (GNS)/CoAl-layered double hydroxide (CoAl-LDH) composite with a laminated structure is fabricated by a simple refluxing method. It is found that CoAl-LDH lamellar crystallites gradually self-assemble on the graphene oxide (GO) which is reduced to GNS during the refluxing procedure in the presence of urea. The GNS/CoAl-LDH composite has a higher specific surface area (23.4 $m^2\,g^{-1}$) and superior electrochemical performance. As electrode material for supercapacitors, the composite shows a maximum specific capacitance of 711.5 $F\,g^{-1}$ at low current density of 1 $A\,g^{-1}$, and it remains 516.8 $F\,g^{-1}$ when the current density increase to 10 $A\,g^{-1}$. Furthermore, the capacitance keeps at least about 81% (compare with 64% for that of pure LDH) after 2000 cycles at 10 $A\,g^{-1}$, indicating the composite has excellent high-current capacitive behavior.

1. Introduction

Supercapacitors, also known as electrochemical capacitors or ultracapacitors, have attracted tremendous attention over the past few years because of their higher energy densities by orders of magnitude than conventional capacitors and greater power densities, and longer cycle life compared to secondary batteries [1–4]. In general, supercapacitors can be classified into two types according to their energy storage mechanism [1]: electrical double layer capacitor and pseudocapacitors, depending on whether Faradaic redox reactions exits or not during the charge and discharge process. So far, there have been a few kinds of electrode materials including carbon materials [2] used as the electrodes of double layer capacitor and conducting polymers [5], metal oxides [6,7] or hydroxides [8,9] which are corresponding to pseudocapacitors. In order to exploit the potential of supercapacitors, more work has been devoted to improve the performance of electrode materials.

As one of supercapacitor electrode materials, layered double hydroxides (LDHs) with a general formula of $[M_{1-x}^{2+}M_x^{3+}(OH)_2](A_{x/n}^{n-})\cdot mH_2O$ [10] have attracted tremendous attention, where M^{2+} and M^{3+} are divalent and trivalent cations and A^{n-} can be an interlayer anion. Because of the flexible ion-exchangeability and tunable composition, LDHs have a series of important applications in catalysts or catalyst precursors, anion exchangers, precursors to other materials, etc. [11–15]. In electrochemical field, LDHs are promising for next-generation supercapacitors in which electrical double layered capacitance and Faradaic pseudocapacitance can be simultaneously acquired because of their abundant slabs and electrochemically active sites [16]. Recently, Zhang and co-workers studied the electrochemical properties of CoAl-LDH as electrode material for supercapacitor [17–20]. Wang et al. reported electrodes of NiAl-LDH coated on the surface of nickel foam which displayed a specific capacitance of 701 $F\,g^{-1}$ at a current density of 10 $mA\,cm^{-1}$ [21]. However, the relative low conductivity constrains electron transfer, resulting in poor high-rate charge and discharge capability and consequently impacts the performance of electrode materials. Thus, a hybrid electrode architecture which incorporates LDH on a high-surface-area conductive support is thought as an ideal method to optimize for the electrochemical performance. LDH synthesized by potentiostatic deposition showed better electrochemical performance but it was unsuited to mass production [22,23]. Zhang et al. mixed multiwalled carbon nanotubes with CoAl-LDH and found that the specific capacitance and long-life performance of the composite at high current density was superior to pure LDH electrode [24]. Activated carbon/LDH composite electrodes have also been reported to retain the value of specific capacitance after long cycling at high current density [25].

Nowadays, graphene, a single layer of carbon atoms with a two-dimensional structure, has attracted intense interest all over the world owing to its intriguing properties [26–29]. Graphene oxide (GO), one of the most important derivatives of graphene, performs

* Corresponding author. Tel.: +86 025 52112918; fax: +86 025 52112626.
E-mail addresses: azhangxg@163.com, azhangxg@nuaa.edu.cn (X. Zhang).

0378-7753/$ – see front matter © 2011 Elsevier B.V. All rights reserved.
doi:10.1016/j.jpowsour.2011.10.056

a layered structure with oxygen functional groups bearing on the basal planes and edges which render GO hydrophilic and highly dispersible in water [30,31]. Therefore, the stable flexible GO is often used as starting material for the preparation of GO-based or GNS-based hybrid materials after reducing [32–39]. In general, the hybrid materials of GNS combined with nanoparticles are expected to improve the prospects for electrochemical applications. On the one hand, the ultrathin flexible GNS have an excellent electrical conductivity and provide a support for anchoring well-dispersed particles. On the other hand, the particles on GNS can effectively prevent the agglomeration of GNS and obtain a higher active surface area which is a decisive factor for electrode materials.

Herein, a simple approach for the fabrication of GNS/CoAl-LDH composites is developed by refluxing process in one-pot for the first time, where CoAl-LDH crystallites anchor on the conducting GNS. The cobalt cations formed by the ionization of metal salts solution are adsorbed onto the GO sheets, followed by the nucleation and in situ growth of the CoAl-LDH crystallites, and meanwhile, GO is reduced to GNS in the existence of urea. Due to the outstanding properties of GNS and CoAl-LDH aforementioned, the as-prepared GNS/CoAl-LDH composites show excellent electrochemical characteristics as supercapacitor materials with a maximum specific capacitance of 516.8 F g^{-1} at a high current density of 10 A g^{-1} and the capacitance can retain at least about 81% after 2000 cycles.

2. Experimental

2.1. Synthesis of GNS/CoAl-LDH composites

All chemicals used here were analytical grade and used as received without any further treatment. GO was prepared from graphite powder (SP, Sinopharm Chemical Reagent Co. Ltd) using a modified Hummers method [40,41]. GNS/CoAl-LDH composite was prepared via a method of homogeneous precipitation. In a typical procedure, a certain amount of dried GO was suspended in 100 mL of ultrapure water with ultrasonication for 1 h and transferred into a three-necked round-bottom flask. Then, $CoCl_2{\cdot}6H_2O$, $AlCl_3{\cdot}6H_2O$ were dissolved in the above dispersion with stirring for 30 min to give the final concentrations of 10, 5 mM, respectively. Subsequently, urea was added and the mixed solution was refluxed at 95 °C under continuous magnetic stirring for 48 h. After filtering and washing with ultrapure water and ethanol for several times, the resulting precipitant was dried at 50 °C in air overnight. The amount of added GO was 5.5, 11, 22 and 33 mg, and the concentrations of urea were 45, 55, 75 and 95 mM, while GNS content of the final composite was determined by dissolving a weighed amount of GNS/CoAl-LDH material with an aqueous HCl solution. The composites were denoted as GL-1, GL-2, GL-3 and GL-4 respectively, corresponding to the GNS contents of 5.5%, 9.3%, 15.1% and 18.8% after calculating. For comparison, pure CoAl-LDH sheets were prepared in the same conditions using $CoCl_2{\cdot}6H_2O$, $AlCl_3{\cdot}6H_2O$ and urea but without the presence of GO, labeled LDH. To prepare GNS, 22 mg GO dispersed into 100 ml of ultrapure water with ultrasonication for 1 h, and then 240 mg urea was added and the mixed solution was refluxed at 95 °C under continuous magnetic stirring for 48 h.

2.2. Material characterizations

Powder X-ray diffractions (XRD) of the samples were studied by a Bruker D8 Advance X-ray diffractometer using Cu Kα radiation (λ = 0.15406 nm). The Fourier transform infrared spectroscopy (FT-IR) spectra of the samples were tested on a Nicolet 750 Fourier transform infrared spectrometer. The Brunauer–Emmett–Teller (BET) surface area was obtained with a Micromeritics ASAP 2010 analyzer. The morphology and structural properties of the samples were observed on a LEO-1550 field emission scanning electron microscope (FESEM) with an applied voltage of 5 kV and a transmission electron microscope (TEM, JEOL JEM-2100).

2.3. Electrochemical measurements

All the electrochemical measurements were carried out in a conventional three-electrode system with 6 M KOH aqueous solution as the electrolyte at room temperature. Platinum foil and a saturated calomel electrode (SCE) were used as counter and reference electrodes. The working electrodes were prepared by mixing active material (5 mg), acetylene black and polytetrafluorene-ethylene (PTFE) binder with a weight ratio of 80:15:5 and dispersing in water. After coating the above slurries on foamed Ni grids (1 cm × 1 cm), the electrodes were dried at 50 °C for several hours before pressing under a pressure of 20 MPa. A CHI660C electrochemical working station instrument was employed for cyclic voltammetry (CV) and galvanostatic charge/discharge measurements by chronopotentiometry.

3. Results and discussion

Fig. 1 shows the FT-IR spectra of the as-prepared samples. In Fig. 1a, the spectrum of GO illustrates O–H stretching mode at 3400 cm^{-1}, C=O (carboxylic acid) at 1718 cm^{-1}, C=C at 1617 cm^{-1} originated from skeletal vibrations of un-oxidized graphitic domains or the stretching deformation vibration of intercalated water, C–O–C at 1220 cm^{-1} and C–O at 1054 cm^{-1} in epoxy or

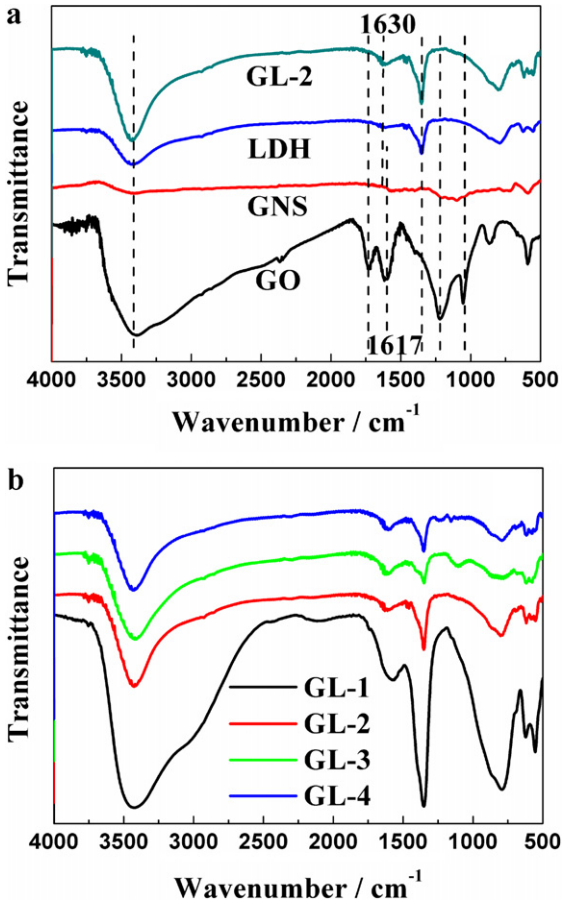

Fig. 1. FT-IR spectra of (a) GO, GNS, LDH, GL-2 and (b) the four composites: GL-1, GL-2, GL-3 and GL-4.

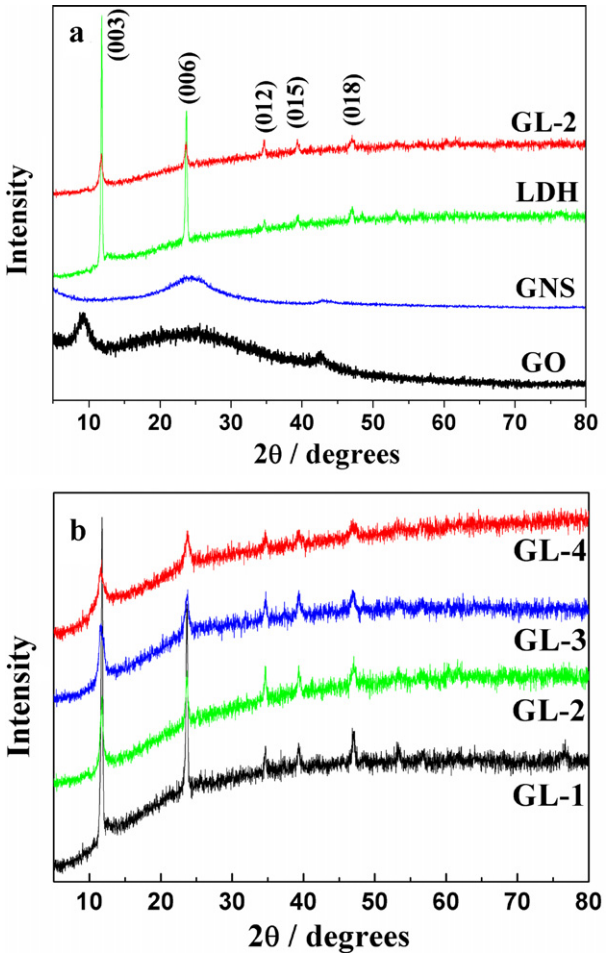

Fig. 2. XRD patterns of (a) GO, GNS, LDH, GL-2 and (b) the four composites: GL-1, GL-2, GL-3 and GL-4.

alkoxy [42]. After treated by urea, the peaks for oxygen functional groups almost disappear except a bit of epoxide and hydroxyl groups. For LDH, the broad peak centered at 3430 cm^{-1} corresponds to the O–H stretching vibration of water molecules in the interlayer and H-bonded OH group, companied with the bending mode at 1630 cm^{-1}. The intense peaks at 1351 and 790 cm^{-1} are ascribed to the ν_3 vibration and bending modes of CO_3^{2-}, respectively. Other absorption bands below 800 cm^{-1} are assigned to metal–oxygen (M–O) stretching and bending modes in the brucite-like lattice. All above observations are concordant with the previous reports [17]. After combination, no significant difference is observed between LDH and GL-2, so are the samples GL-1, GL-3 and GL-4, as shown in Fig. 1b. Similarly, it is found that the characteristic peaks of GO disappear in the four samples. However, with increasing the GO content, not all the functional groups on the surface of GO can be attached to limited positive ions, so one can observe some slight peaks at 1054 cm^{-1} and 1220 cm^{-1} which are due to the remaining alkoxy or epoxy groups of GNS in the finally products, seen from the images of GL-3 and GL-4. The peak at 1617 cm^{-1} was unconspicuous, which may be overlapped by the broad peak at 1630 cm^{-1} originated from the vibrations of the adsorbed water molecules.

The XRD patterns of LDH and the composites are presented in Fig. 2 together with that of GO and GNS. Obviously, GO displays an intense peak of (0 0 2) reflection at $2\theta = 9.1^\circ$ with an interlayer spacing of 0.96 nm that is much larger than that of pristine graphite (0.34 nm), demonstrating the complete oxidation of graphite into GO due to the introduction of oxygen-containing functional groups on the graphite sheets [43]. After reduction in the presence of urea, the peak at 9.1° of GO completely disappears and a broad peak at around $2\theta = 24.4^\circ$ representing an interlayer spacing of 0.36 nm is observed. It can be interpreted in terms of short-range order of the GNS along the stacking direction and the residual functional groups which may be present between the graphene layers [36]. The diffraction pattern of the pristine LDH well corresponds to the standard compound $Co_6Al_2CO_3(OH)_{16}\cdot H_2O$ (JCPDS: 51-0045) with the characteristic peaks of (0 0 3), (0 0 6), (0 1 2), (0 1 5) and (0 1 8) planes. No peaks of impurities are observed. The diffraction peaks of (0 0 3) ($2\theta = 11.8^\circ$) and (006) ($2\theta = 23.7^\circ$) are especially strong, while other peaks have relatively weak intensities, showing that the crystal grew along a certain axis. Furthermore, the interlayer distance is 0.748 nm (d_{003}), indicating the occupying of CO_3^{2-} ions and water molecules in the interlayer spaces [17], which is correspond to the results of FT-IR in Fig. 1a. In comparison, all diffraction peaks observed in the composite GL-2 are still in good accordance with those of LDH, so are the composites GL-1, GL-3 and GL-4; see Fig. 2b. However, the diffraction peaks of graphene are not distinguishable in the composites. The CoAl-LDH crystals deposited on GNS can prevent them from stacking into mutilayers, leading to the much lower crystalline extent of graphene than that of CoAl-LDH, which results in the shielding of the graphene peaks by those of CoAl-LDH [44]. Moreover, as the GNS percentage increases in the composite, the intensities of the peaks for the composites weaken gradually, manifesting the poor crystallization of the GNS/CoAl-LDH materials, which could affect the structure and the performance of the composite.

Fig. 3a presents the representative FESEM image of GNS agglomerate, consisting of almost transparent carbon nanosheets with multilayer, while GO has lots of wrinkles with a lateral dimensions of several micrometers (inset in Fig. 3a). For LDH, the crystals grow along a certain axis undisturbed, so they show a typical lamellar morphology and the sheets are so thin that the CoAl-LDH layers present circles which are actually composed of hexagons with a mean lateral size of several micrometers, seen in Fig. 3b. By contrast, the obtained GNS/CoAl-LDH composites, GL-1 (Fig. 3c), GL-2 (Fig. 3d), GL-3 (Fig. 3e) and GL-4 (Fig. 3f) show laminated structures with CoAl-LDH layers are pinned by the high-concentration oxygen groups and defects on GO without well-defined morphologies. By ultrasonication and refluxing for such a long time, the added GO is exfoliated to plenty of unilaminar flakes to form large amount of restricted spaces. During the refluence procedure, the unilaminar flakes act as matrixes to adsorb metallic ions, followed by the nucleation and growth of the CoAl-LDH crystallites. Because of the existence of the restricted spaces, the CoAl-LDH crystals cannot grow as freely as before but in different directions and gain smaller sheets. Meanwhile, the CoAl-LDH crystals deposited on GNS can prevent them from stacking into multilayers, which maintains the high surface and intrinsic chemical and physical properties of GNS. Finally, a laminated structure combining GNS and CoAl-LDH is formed. It should be pointed out that the combination between ultrathin GNS and CoAl-LDH can form conducting 3D graphene conductive network and porous structure of the GNS/CoAl-LDH composite. The 3D conductive network could increase electronic conductivity of the composite while the porous structure can facilitate liquid electrolyte diffusion into the electrode materials, which is beneficial for achieving high rate performance [45]. To further examine the architecture of GNS/CoAl-LDH composite, the samples are investigated by TEM. Fig. 4a shows the TEM image of GNS which are almost transparent with some wrinkles and entangled with each other. However, for the sample GL-2 in Fig. 4b, the image is just composed of many flakes with different sizes and irregular shapes. The flakes stack with each other, so it is hard to see scrolled GNS except some area the GNS can be observed (inset in Fig. 4b).

N_2 adsorption/desorption isotherms are performed to examine the pore structures of LDH and GL-2 (shown in Fig. 5) and the

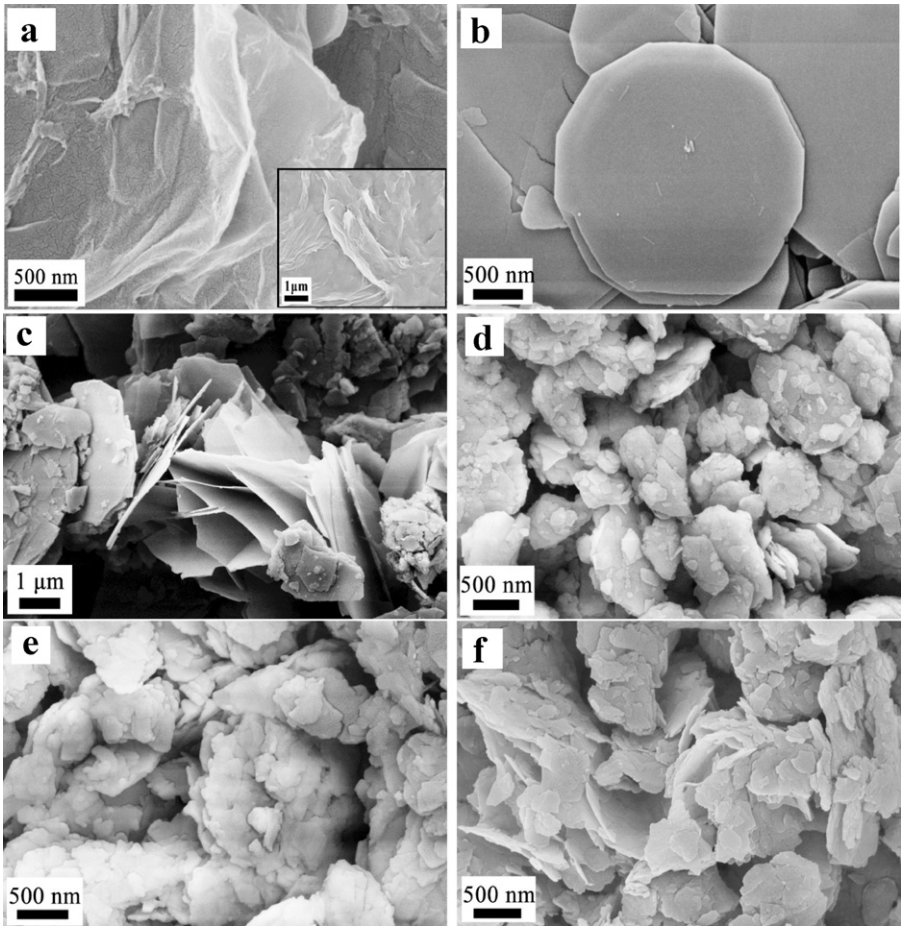

Fig. 3. Typical FESEM images of (a) GNS, (b) LDH, (c) GL-1, (d) GL-2, (e) GL-3 and (f) GL-4.

specific textural properties are presented in Table 1. Owing to the addition of GNS, CoAl-LDH crystals with smaller sizes form and more surfaces get exposed, so it can be obviously seen that the BET specific surface area of the composite ($23.4\,m^2\,g^{-1}$) is higher than that of pure LDH ($7.1\,m^2\,g^{-1}$), resulting in more excellent electrochemical characteristics for GL-2. Moreover, the total pore volume of GL-2 increases, from $0.04\,cm^3\,g^{-1}$ of pure LDH to $0.10\,cm^3\,g^{-1}$. The increased pore volume maybe attribute to the formation of secondary pores between the GNS and CoAl-LDH crystals, providing efficient transport pathways to their interior voids, which is critical for high-rate LDHs application.

Based on the above analysis, a proposed route for the preparation of the GNS/CoAl-LDH composites are shown in Scheme 1. When natural graphite is oxidized to GO by using Hummers method, there are abundant functional groups (–OH, –COOH, etc.) on the surface of GO acting as anchor sites for the in situ growth of crystal. Positive Co^{2+} ions, formed by the ionization of $CoCl_2{\cdot}6H_2O$ in water, firstly attach to the negatively charged functional groups on GO by electrostatic attraction and serve as nucleation precursors. In the presence of $AlCl_3{\cdot}6H_2O$ and urea, a mass of nuclei form and the as-prepared CoAl-LDH crystals adhere to the surface of GO via an intermolecular hydrogen bond or a covalent coordination bond. As the reaction goes on, GO is reduced to GNS which hinders the agglomeration and growth of CoAl-LDH lamellar crystallites, which in turn results in the exfoliation of GNS, and finally obtain a lamination structure for rapid electronic and ionic transport.

Table 1
Specific surface area, pore volume for the samples LDH and GL-2.

Samples	S_{BET} ($m^2\,g^{-1}$)	V_{pores} ($cm^3\,g^{-1}$)
LDH	7.1	0.04
GL-2	23.4	0.10

The cyclic voltammograms of the samples characterized at a scan rate of $5\,mV\,s^{-1}$ in 6 M KOH solution are presented in Fig. 6. Fig. 6a shows the CV curves of Ni grid, LDH and GL-2 with a potential range of 0–0.55 V (vs. SCE). It is found that the foamed Ni grid exhibits a redox process with low current intensities. This is mainly related to the reversible reactions of Ni(II)/Ni(III) cause by the existence of nickel oxide on the surface of nickel grid. For composite electrodes, in Fig. 6b, the CV shapes are basically the same as LDH (Fig. 6a), and a set of redox waves observed obviously at the potential of 410 mV and 255 mV indicate the existence of the Faradaic process, which is attributed to the conversion of Co(II)/Co(III). The redox reaction can be written as follows [17], where HT stands for hydrotalcite-like compound:

$$HT - Co(II) + OH_{sol}{}^{-} \Leftrightarrow HT(OH^{-}) - Co(III) + e^{-}$$

Moreover, the integral area of the CV curve for GL-2 is the largest, suggesting the highest electrochemical capacitance.

As illustrated in Fig. 7, galvanostatic charge/discharge measurements of the as-prepared composites are carried out in 6 M KOH in the potential range of 0–0.5 V at different current densities. As can be seen, the charge/discharge curves are not ideal straight lines, also confirming the Faradaic reaction is proceeding. The specific capacitance (C_s) of the composites calculated from Eq. (1) is listed in Table 2 and more intuitive information is shown in Fig. 8. It can be found that C_s decreases with the increase of current densities from

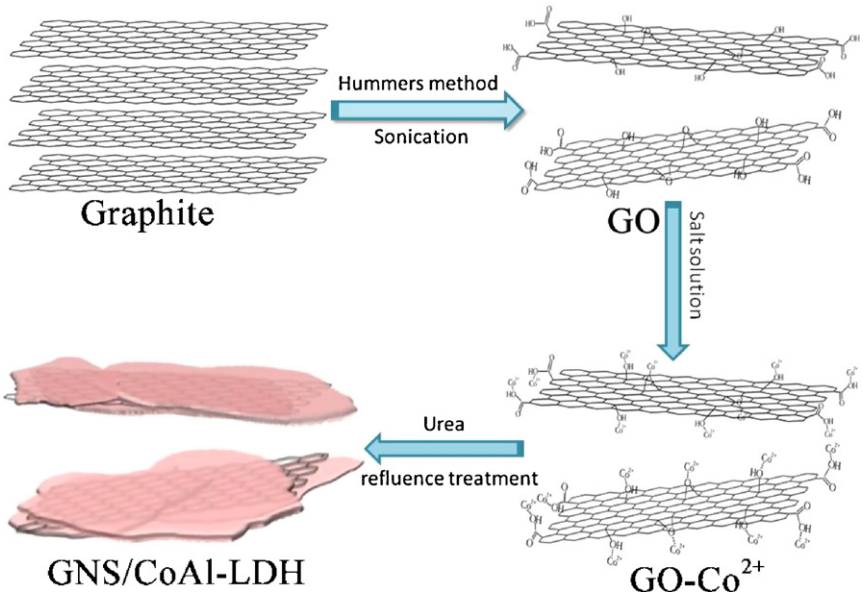

Scheme 1. Schematic illustration of the synthesis process for the GNS/CoAl-LDH composites.

1 to 10 A g^{-1}. At a low current density, almost all the active surface area of electrode can contact well with the electrolyte ions to react completely, leading to a higher C_s. However, at high current density, the effective interaction between the ions and the electrode is greatly reduced, so the capacitance decreases.

In addition, the C_s of GL-2 and GL-3 are higher than that of pure LDH and the retention rates of all GNS/CoAl-LDH composites are higher than that of pure LDH. That is because the addition of GNS can work as a highly conductive matrix for quickly providing

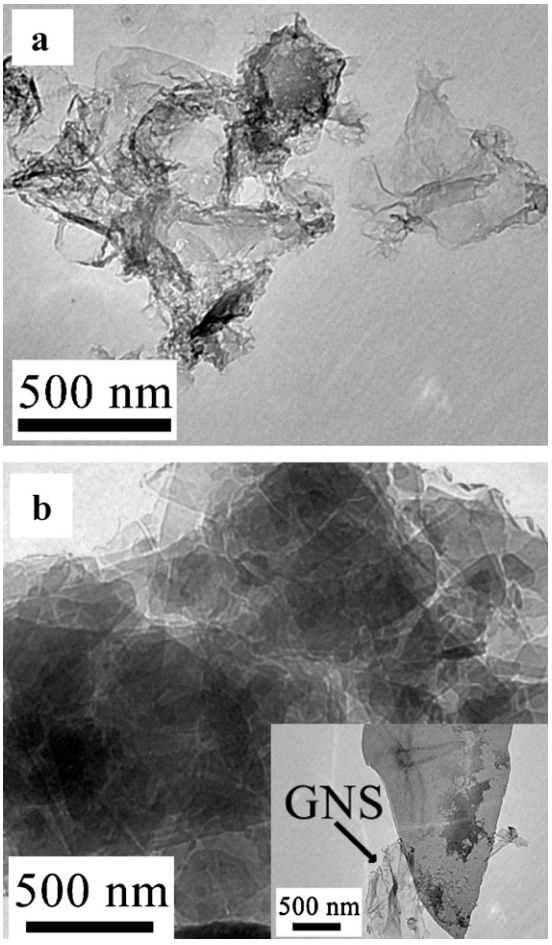

Fig. 4. TEM images of (a) GNS and (b) GL-2.

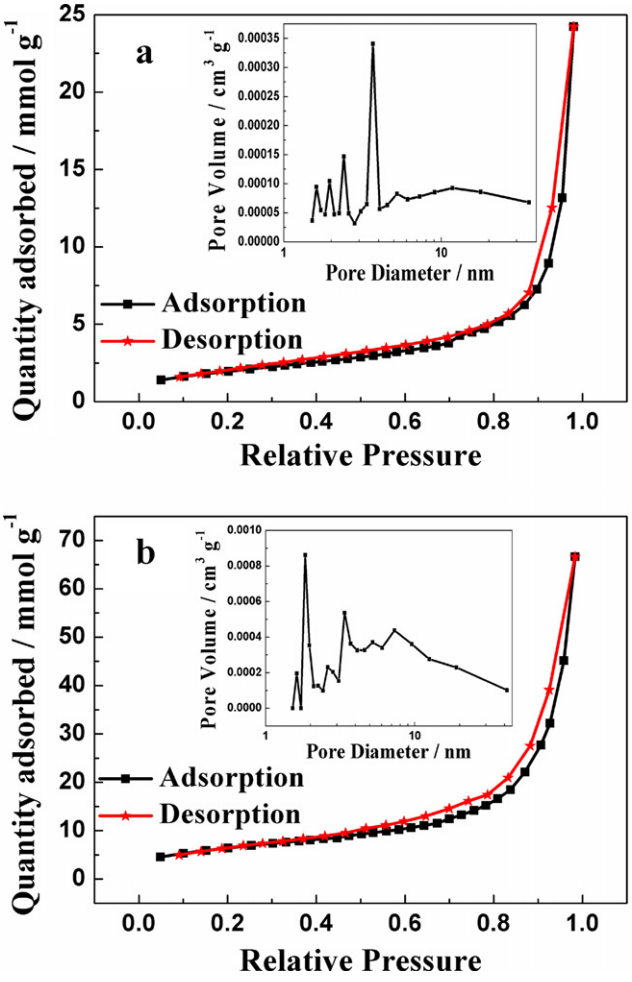

Fig. 5. The gas (N_2) adsorption–desorption isotherm loop and the pore size distribution data for the synthesized LDH (a) and GL-2 (b).

Table 2
Specific capacitance of the samples at various current densities.

Current density ($A g^{-1}$)	LDH (C_s: $F g^{-1}$)	GL-1 (C_s: $F g^{-1}$)	GL-2 (C_s: $F g^{-1}$)	GL-3 (C_s: $F g^{-1}$)	GL-4 (C_s: $F g^{-1}$)
1	641.2	623.8	711.5	672.3	585.2
10	421.4	443.8	516.8	491.9	407.9
Retention rate	65.7%	71.1%	72.6%	73.2%	69.7%

electrons to CoAl-LDH to improve high-current capacitive performance. Especially, the sample GL-2 shows the best electrochemical properties with a maximum C_s of 711.5 $F g^{-1}$ obtained at a current density of 1 $A g^{-1}$, and 516.8 $F g^{-1}$ even at 10 $A g^{-1}$ with a retention rate of 72.6%, which is higher than 65.7% of pure LDH. After correction for the weight percentage of the redox-active phase of LDH, a maximal corrected C_s of ca. 791.9 $F g^{-1}$ at 1 $A g^{-1}$ and 579.4 $F g^{-1}$ at 10 $A g^{-1}$ for LDH of the composite GL-3 with 15.1 wt.% GNS loading. Moreover, as shown in the inset in Fig. 8, further increase or decrease of GNS loading both result in a decrease in corrected C_s. When GNS loading is more than 15.1%, it would cause the decrease of electroactive sites, leading to the decrease of C_s of the composite. It also implies that when the GNS loading is less than 15.1%, it does not favor the formation of effectively dispersed CoAl-LDH layers on GNS and finally results in the low utilization of CoAl-LDH. However, such corrected C_s values are still higher than that of the pure LDH.

$$C_s = \frac{I\Delta t}{m\Delta V} \quad (1)$$

Furthermore, the electrochemical stability of the five samples with a range of 0–0.5 V at 10 $A g^{-1}$ in 6 M KOH solution for 2000 cycles is shown in Fig. 9. It is found that the GNS/CoAl-LDH electrodes exhibit more excellent long cycle life over the entire cycle numbers. While for the four composites, there are slight decreases in the initial 200 or 300 cycle tests and after the following 1700 or 1800 cycles, the capacitance almost remain unchangeable. After 2000 cycles, the GL-1, GL-2, GL-3 and GL-4 retain about 77% (400.3 $F g^{-1}$), 81.2% (519.8 $F g^{-1}$), 89.7% (519.8 $F g^{-1}$) and 88% (440 $F g^{-1}$) of their initial capacitance, respectively, while the

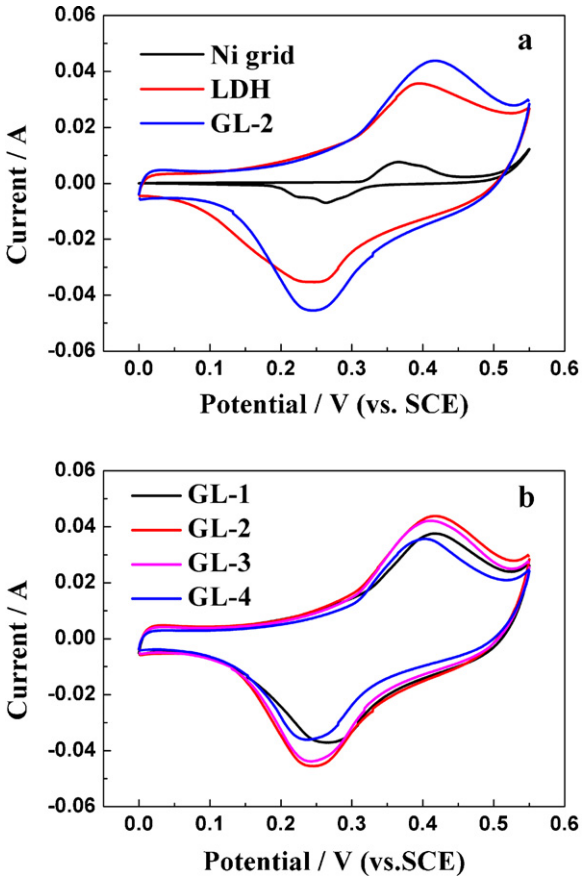

Fig. 6. Cyclic voltammograms of (a) Ni grid, LDH, GL-2 and (b) GL-1, GL-2, GL-3, GL-4 at 5 $mV s^{-1}$ in 6 M KOH aqueous solution.

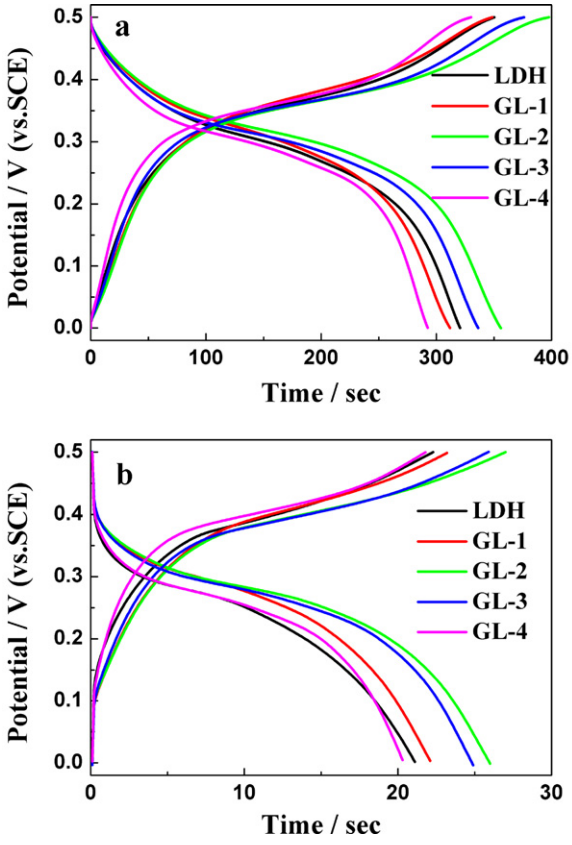

Fig. 7. The charge/discharge curves of LDH, GL-1, GL-2, GL-3 and GL-4 at (a) 1 $A g^{-1}$ and (b) 10 $A g^{-1}$.

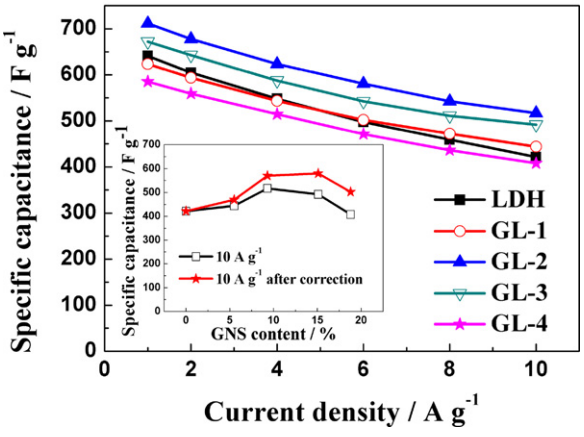

Fig. 8. Specific capacitance of the samples at different current densities.

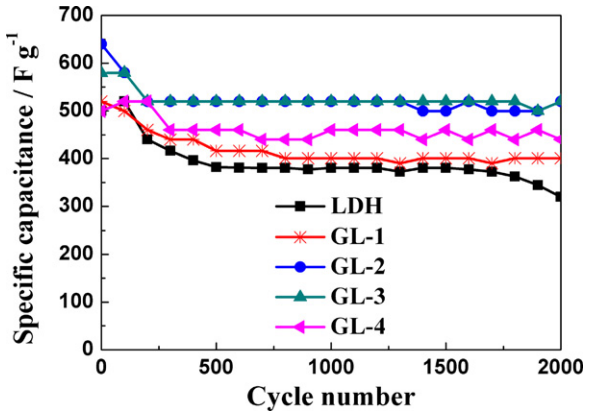

Fig. 9. The cycle life of LDH, GL-1, GL-2, GL-3 and GL-4 at 10 A g^{-1} in 6 M KOH solution.

specific capacitance of pure LDH is only 319.7 F g^{-1} (decreases more than 36%). The superior electrochemical performance of GNS/CoAl-LDH composites especially the enhanced high-current capacitive behavior may be attributed to the aspects as follows: firstly, the presence of GNS results in the formation of smaller sizes CoAl-LDH lamellas which in turn reduce the degree of restacking of GNS, and consequently increase the effective interfacial area between the CoAl-LDH and electrolyte to improve the electrochemical utilization of CoAl-LDH. Secondly, the GNS in the composites have a good electrical conductivity and provide a conductive network for electron transport during the electrode reaction process, which is favorable for stabilizing the electronic and ionic conductivity, therefore leading to a higher specific capacity. Thirdly, the hybridization between ultrathin GNS and CoAl-LDH can form secondary pores providing some extra pore volume, which is beneficial for achieving high rate performance. Finally, as flexible 2-D carbon supports for anchoring CoAl-LDH lamellar crystallites, GNS in the prepared composites can efficiently prevent the aggregation of CoAl-LDH during continuous cycling.

In summary, the excellent electrochemical performance of the overall electrodes can be attributed to the synergetic effect between conducting GNS and CoAl-LDH crystallites. Therefore, the synthesized composites could have some practical applications as electrodes for electrochemical capacitor.

4. Conclusions

GNS/CoAl-LDH composites were firstly successfully synthesized by a simple and facile method, showing higher specific capacitance, better rate capability and cycling stability as supercapacitor electrodes. The CoAl-LDH crystals adhered to the surface of GNS to form laminated structure with smaller size compared with the pure CoAl-LDH, which facilitate electrolyte soaking into electrode materials. Owing to the combined advantages of conducting GNS and CoAl-LDH crystallites, the hybrid electrode materials show superior electrochemical properties at a high current density. Further optimization and control of the structures to exploit better electrochemical properties of graphene-based composites are under investigation in our group.

Acknowledgements

This work was supported by National Basic Research Program of China (973 Program) (No. 2007CB209703), National Natural Science Foundation of China (No. 20873064).

References

[1] B.E. Conway, J. Electrochem. Soc. 138 (1991) 1539–1540.
[2] E. Frackowiak, F. Beguin, Carbon 39 (2001) 937–950.
[3] P. Simon, Y. Gogotsi, Nat. Mater. 7 (2008) 845–854.
[4] C. Liu, F. Li, L.P. Ma, H.M. Cheng, Adv. Mater. 22 (2010) E28–E62.
[5] K. Zhang, L.L. Zhang, X.S. Zhao, J. Wu, Chem. Mater. 22 (2010) 1392–1401.
[6] C.Z. Yuan, L. Chen, B. Gao, L.H. Su, X.G. Zhang, J. Mater. Chem. 19 (2009) 246–252.
[7] B. Gao, C.Z. Yuan, L.H. Su, S.Y. Chen, X.G. Zhang, Electrochim. Acta 54 (2009) 3561–3567.
[8] S.C. Tang, S. Vongehr, Y. Wang, L. Chen, X.K. Meng, J. Solid State Chem. 183 (2010) 2166–2173.
[9] J.K. Chang, C.M. Wu, I.W. Sun, J. Mater. Chem. 20 (2010) 3729–3735.
[10] F. Cavani, F. Trifiro, A. Vaccari, Catal. Today 11 (1991) 173–301.
[11] H. Wang, X. Xiang, F. Li, AIChE J. 56 (2010) 768–778.
[12] Z.P. Liu, R.Z. Ma, M. Osada, N. Iyi, Y. Ebina, K. Takada, T. Sasaki, J. Am. Chem. Soc. 128 (2006) 4872–4880.
[13] G. Abellan, E. Coronado, C. Marti-Gastaldo, E. Pinilla-Cienfuegos, A. Ribera, J. Mater. Chem. 20 (2010) 7451–7455.
[14] J.B. Han, D.P. Yan, W.Y. Shi, J. Ma, H. Yan, M. Wei, D.G. Evans, X. Duan, J. Phys. Chem. B 114 (2010) 5678–5685.
[15] Y. Cao, Y. Zhao, Q.X. Li, Q.Z. Jiao, J. Chem. Sci. 121 (2009) 225–229.
[16] X.M. Liu, Y.H. Zhang, X.G. Zhang, S.Y. Fu, Electrochim. Acta 49 (2004) 3137–3141.
[17] L.H. Su, X.G. Zhang, J. Power Sources 172 (2007) 999–1006.
[18] L.H. Su, X.G. Zhang, C.H. Mi, Y. Liu, J. Power Sources 179 (2008) 388–394.
[19] L.H. Su, X.G. Zhang, C.Z. Yuan, B. Gao, J. Electrochem. Soc. 155 (2008) A110–A114.
[20] L.H. Su, X.G. Zhang, C.H. Mi, B. Gao, Y. Liu, Phys Chem. Chem. Phys. 11 (2009) 2195–2202.
[21] J. Wang, Y.C. Song, Z.S. Li, Q. Liu, J.D. Zhou, X.Y. Jing, M.L. Zhang, Z.H. Jiang, Energy Fuels 24 (2010) 6463–6467.
[22] V. Gupta, S. Gupta, N. Miura, J. Power Sources 175 (2008) 680–685.
[23] V. Gupta, S. Gupta, N. Miura, J. Power Sources 177 (2008) 685–689.
[24] L.H. Su, X.G. Zhang, Y. Liu, J. Solid State Electrochem. 12 (2008) 1129–1134.
[25] A. Malak-Polaczyk, C. Vix-Guterl, E. Frackowiak, Energy Fuels 24 (2010) 3346–3351.
[26] D. Li, M.B. Muller, S. Gilje, R. Kaner, G.G. Wallace, Nat. Nano. 3 (2008) 101–105.
[27] Z.S. Wu, W.C. Ren, L.B. Gao, B.L. Liu, C.B. Jiang, H.M. Cheng, Carbon 47 (2009) 493–499.
[28] X.L. Li, G.Y. Zhang, X.D. Bai, X.M. Sun, X.R. Wang, E.G. Wang, H.J. Dai, Nat. Nano. 3 (2008) 538–542.
[29] A.K. Geim, K.S. Novoselov, Nat. Mater. 6 (2007) 183–191.
[30] H.K. Jeong, Y.P. Lee, R.J.W.E. Lahaye, M.H. Park, K.H. An, I.J. Kim, C.W. Yang, C.Y. Park, R.S. Ruoff, Y.H. Lee, J. Am. Chem. Soc. 130 (2008) 1362–1366.
[31] T. Szabo, O. Berkesi, P. Forgo, K. Josepovits, Y. Sanakis, D. Petridis, I. Dekany, Chem. Mater. 18 (2006) 2740–2749.
[32] Z.S. Wu, D.W. Wang, W.C. Ren, J.P. Zhao, G.M. Zhou, F. Li, H.M. Cheng, Adv. Funct. Mater. 20 (2010) 3595–3602.
[33] D.H. Wang, R. Kou, D. Choi, Z.G. Yang, Z.M. Nie, J. Li, L.V. Saraf, D.H. Hu, J.G. Zhang, G.L. Graff, J. Liu, M.A. Pope, I.A. Aksay, ACS Nano 4 (2010) 1587–1595.
[34] Y.S. He, D.W. Bai, X.W. Yang, J. Chen, X.Z. Liao, Z.F. Ma, Electrochem. Commun. 12 (2010) 570–573.
[35] Z.S. Wu, W.C. Ren, L. Wen, L.B. Gao, J.P. Zhao, Z.P. Chen, G.M. Zhou, F. Li, H.M. Cheng, ACS Nano 4 (2010) 3187–3194.
[36] J. Yan, T. Wei, W.M. Qiao, B. Shao, Q.K. Zhao, L.J. Zhang, Z.J. Fan, Electrochim. Acta 55 (2010) 6973–6978.
[37] H.J. Li, G. Zhu, Z.H. Liu, Z.P. Yang, Z.L. Wang, Carbon 48 (2010) 4391–4396.
[38] S.M. Paek, E. Yoo, I. Honma, Nano Lett. 9 (2009) 72–75.
[39] H.L. Wang, H.S. Casalongue, Y.Y. Liang, H.J. Dai, J. Am. Chem. Soc. 132 (2010) 7472–7477.
[40] W.S. Hummers, R.E. Offeman, J. Am. Chem. Soc. 80 (1958) 1339–1340.
[41] N.I. Kovtyukhova, P.J. Ollivier, B.R. Martin, T.E. Mallouk, S.A. Chizhik, E.V. Buzaneva, A.D. Gorchinskiy, Chem. Mater. 11 (1999) 771–778.
[42] W.N. Zhang, W. He, X.L. Jing, J. Phys. Chem. B 114 (2010) 10368–10373.
[43] Z.H. Liu, Z.M. Wang, X. Yang, K. Ooi, Langmuir 18 (2002) 4926–4932.
[44] Z.F. Du, X.M. Yin, M. Zhang, Q.Y. Hao, Y.G. Wang, T.H. Wang, Mater. Lett. 64 (2010) 2076–2079.
[45] P.C. Lian, X.F. Zhu, S.Z. Liang, Z. Li, W.S. Yang, H.H. Wang, Electrochim. Acta 56 (2011) 4532–4539.